

Thermal conductance of a diffusive NSN wire probed by shot noise

A.V. Bubis,^{1,2} E.V. Shpagina,^{2,3} A.G. Nasibulin,^{1,4} and V.S. Khrapai^{2,3}

¹*Skolkovo Institute of Science and Technology, Nobel street 3, 121205 Moscow, Russian Federation*

²*Institute of Solid State Physics, Russian Academy of Sciences, 142432 Chernogolovka, Russian Federation*

³*National Research University Higher School of Economics, 20 Myasnitskaya Street, Moscow 101000, Russia*

⁴*Aalto University, P. O. Box 16100, 00076 Aalto, Finland*

We investigate diffusive nanowire-based structures with two normal terminals on the sides and a central superconducting island in the middle, which is either grounded or floating. Using a semiclassical calculation we demonstrate that both device layouts permit a quantitative measurement of the energy-dependent sub-gap thermal conductance G_{th} from the spectral density of the current noise. In the floating case this goal is achieved without the need to contact the superconductor provided the device is asymmetric, that may be attractive from the experimental point of view. Our calculations are directly applicable to the multi-mode case and can serve as a starting point to understand the shot noise response in open one dimensional Majorana device.

I. INTRODUCTION

Electronic transport in hybrid semiconductor-superconductor devices is getting a second breath in the context of recent topological band theory. One of the promising directions is a realization of topological superconductivity in a proximitized semiconducting nanowire (NW) [1, 2], accompanied by emerging Majorana zero modes (MZMs) localized at its ends [3]. While all the prerequisites for this noble goal are there, including ballistic single-mode transport [4], strong spin-orbit coupling [5] and thin superconducting shell capable to withstand strong magnetic fields [6], the non-local character of the proposed MZMs remains to be proved.

The MZMs non-locality can be probed with nonlocal conductance measurements in normal-superconductor-normal (NSN) NW devices [7–9]. Such a three-terminal setup approach allows to overcome the problem of superconducting shell shunting the quasiparticle charge transport and can capture the MZMs via end-to-end conductance correlations [10] and Andreev rectification effect [11]. Alternative to charge transport are nonlocal thermal conductance and shot noise measurements, which provide a universal signature of the topological phase transition even in presence of a moderate disorder [12]. At further increasing the disorder, the thermal conductance becomes the only measure of the non-local quasiparticle response [13]. In the absence of heat transfer through the superconducting shell, one can expect the thermal conductance to be informative also in NSN devices with a floating S-island [14]. Possible relation to the shot noise measurements in such structures remains, however, unknown [15].

A correspondence between the shot noise and thermal conductance is a generic effect not limited to the Majorana case. A doubling of the shot noise in disordered NS junctions [16, 17] is fundamentally related to the suppressed heat transfer in the S-lead [18, 19], and can be useful to probe the sub-gap density of states in such structures [20, 21]. In NSN NW-based devices the shot noise and thermal conductance are directly re-

lated in the limit of charge neutral quasiparticle transport, that was demonstrated in a recent experiment set up in a trivial superconducting phase [22]. It is instructive to trace the interplay of disorder scattering and Andreev reflection in the framework of semiclassical multi-mode NSN devices. By mixing quasiparticle trajectories traversing the proximity region at different angles the disorder randomizes the number of Andreev reflections (ARs) of a sub-gap quasiparticle from the superconducting shell [22, 23]. Since each AR process inverts the quasiparticle charge [24], statistically this favors the charge neutrality of the quasiparticle population. In addition, moderate disorder may enhance the heat conductance by promoting the escape of retro-reflected quasiparticles from poorly propagating trajectories [23, 25]. Thus diffusive multi-mode NSN structures represent a perfect test bed of the relation between the shot noise and thermal conductance.

Here, we investigate a diffusive NSN device in a semiclassical approach of Nagaev and Büttiker [18, 19] and demonstrate the opportunity to extract thermal conductance from the shot noise measurements. We consider two different layouts widely used in Majorana setups with a central superconducting island either connected to a grounded macroscopic terminal or floating. Grounding the superconductor turns it into a perfect charge sink, that is a crucial distinction between these cases. In the grounded case the nonlocal shot noise is sensitive to the thermal conductance of the proximitized section. In the floating case the impact of the thermal conductance on the shot noise is weaker and depends on the device asymmetry. Our results make the floating island geometry considerable for experimentalists, since a technically challenging step of contacting the thin superconducting shell [6, 26–28] can be omitted in this case.

II. SEMICLASSICAL MODEL

We consider a diffusive nanowire (NW) connected to two normal reservoirs (N) and a superconducting contact in the middle (S), which divides the wire in two

normal sections with the resistances r_L and r_R (see the first row in Fig. 1). The normal NW segments on both sides of the S contact are assumed to be much longer than the superconducting coherence length and the applied voltage is much higher than the Thouless energy, $L \gg \sqrt{\hbar D/eV}, \sqrt{\hbar D/\Delta}$, where D is the diffusion coefficient. This allows to neglect the penetration of the superconducting condensate from the proximity region underneath the S contact into the normal segments and treat them as metallic diffusive conductors [18, 19]. The length of the S segment (the part of the device consisting of a part of NW and S contact above it) is assumed to be much larger than both the NW diameter and the superconducting coherence length, which enables to us to describe the quasiparticle transport via this segment as effectively one-dimensional and neglect the processes of Cooper pair splitting and elastic cotunneling [29]. S/NW interface quality is assumed to be nearly ideal, so that the probability of the AR by far exceeds that of the normal quasiparticle reflection. Inelastic scattering in the NW and in the S island is absent. The thermal conductance G_{th} of the S segment is assumed to be finite at energies below the superconducting gap Δ . Above the gap, the S contact shunts both electrical and thermal currents, thus in this energy range the thermal conductance is much larger than that of the adjacent normal NW segments and assumed to be infinite. Throughout the paper we define the thermal conductance similarly to the electrical conductance as $G_{\text{th}} \equiv e^2 \nu^* D^* A/L$, where e is the elementary charge and ν^* , D^* are, respectively, the density of states and diffusion coefficient of the sub-gap quasiparticles in the S segment, A is the cross-section of the NW and L is the length of the S segment. This choice is convenient for our purpose of solving a non-equilibrium finite-bias problem. Note that in general G_{th} may depend on energy owing to the superconducting proximity effect, as we address in the last section of the paper.

In the following we consider two possible realizations of the NSN devices (see schematic device configurations in Fig. 1), with the central S segment either being a part of a grounded superconducting terminal (reservoir) or a floating island. These layouts are referred to, respectively, as the Grounded and the Floating cases. The Grounded case corresponds to a three-terminal NSN device for which the bias voltage V is applied to the left N terminal, whereas the S terminal and the right N terminal are grounded. Corresponding chemical potentials are $\mu_L = -eV$, $\mu_S = 0$ and $\mu_R = 0$. The Floating case corresponds to a two-terminal NSN device for which, without the loss of generality, we also choose the chemical potential of the S segment equal to zero $\mu_S = 0$, therefore $\mu_L = -eV r_L/(r_L + r_R)$ and $\mu_R = eV r_R/(r_L + r_R)$.

Before going into the details of our calculation, we overview the underlying physics of the NSN structure in a few representative cases at a zero bath temperature and finite bias in Fig. 1. Blue arrows in the upper sketches indicate the propagation of the electric current I . The key difference between both device configurations is that

the electric current I flows only through the left NS segment in the Grounded case and through the whole device in the Floating case. Note that in the latter case the current in the S segment is carried by the Cooper condensate and flows predominantly inside the superconductor. The propagation of current has obvious consequences for the local chemical potential μ , see the spatial profiles of both quantities in respective panels of Fig. 1. This and other data are the results of the calculations with the parameters mentioned in the caption. Non-equilibrium sub-gap quasiparticles gain energy from the electric field and propagate diffusively along the NW, relaxing in one of the N terminals. The direction of the heat flux is indicated by the red arrows. Finite G_{th} enables non-equilibrium quasiparticles to traverse the S segment and results in a non-zero heat flux \dot{Q} in the S segment. The spatial dependence of the heat flux is shown in the corresponding panel of Fig. 1. Note that in general \dot{Q} changes sign somewhere in the middle of the NSN device and depends on coordinate, which is a consequence of the Joule heating released in the normal segments that relaxes in the N terminals. In the limit of $G_{\text{th}} = 0$ shown by orange lines, as well as in the special case of symmetric Floating NSN device, the heat flux via the S segment vanishes and the two normal segments completely decouple. Non-equilibrium quasiparticle populations which build up in the biased NSN NW are characterized by coordinate-dependent electronic energy distributions (EEDs) $f(\varepsilon)$, which we calculate in the next section. Relevant to the shot noise measurements in diffusive conductors is the notion of the noise temperature $T_N = (k_B)^{-1} \int f(1-f)d\varepsilon$,

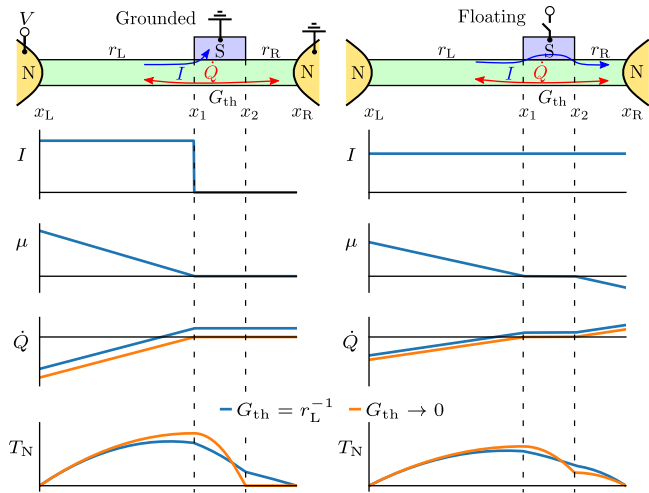


FIG. 1. Schematics of the two NSN device configurations and coordinate dependencies of the key physical quantities: I – electrical current, μ – local chemical potential, \dot{Q} – heat flux integrated over energy, T_N – local noise temperature. The boundaries of the S segment are marked by vertical dashed lines. The parameters used for calculations are $r_L = 6 \text{ k}\Omega$, $r_R = 2 \text{ k}\Omega$, $T = 0$, $|eV| < \Delta$.

which is a measure of local non-equilibrium. The lower panels of Fig. 1 demonstrate the spatial profiles of the T_N . Note that in the limit of $G_{\text{th}} = 0$ the right N segment remains in equilibrium in the Grounded case, whereas it acquires a finite $T_N > 0$ in the Floating case.

III. ENERGY DISTRIBUTIONS

Following the semiclassical approach of Nagaev and Büttiker [18, 19] we calculate the EEDs $f_1(\varepsilon)$ and $f_2(\varepsilon)$ on the two boundaries of the S segment at $x = x_1$ and $x = x_2$, see Fig. 1. The vicinity of the superconductor imposes an important constraint on the EED at sub-gap energies. For the case of a perfect lateral interface between the superconductor and the NW, which is assumed below, AR is the only process of quasiparticle scattering from the interface. Since the number of AR in the diffusive case is a random quantity [22], statistically this results in equal amounts of the electron-like and hole-like sub-gap quasiparticles in the S segment, that is the function $f(\varepsilon, x)$ for $x \in [x_1, x_2]$ obeys the relation $f(\varepsilon, x) = 1 - f(-\varepsilon, x)$. Note that this symmetry automatically guarantees that the chemical potential of the sub-gap quasiparticles coincides with that of the Cooper pairs, i.e. $\mu(x) = 0$.

At sub-gap energies the electric current in the S segment is carried by the Cooper condensate, therefore the conservation of electric current cannot be used to set the boundary conditions for the EED. The proper boundary conditions for $|\varepsilon| \leq \Delta$ are obtained from the conservation of a partial heat flux at a given energy. We define such a heat flux as $\delta\dot{Q}(\varepsilon, x) = -\nu(\varepsilon)D(\varepsilon)[\varepsilon - \mu(x)]\nabla f(\varepsilon, x)\delta\varepsilon$, where $\nu(\varepsilon)$ and $D(\varepsilon)$ are the density of states, diffusion coefficient and chemical potential at this energy and $\delta\varepsilon$ is the width of infinitesimal energy window. Having in mind that AR mixes the two types of quasiparticles in our hybrid system, we observe that the correct conserved quantity is the sum of the partial heat fluxes carried by the electron-like and hole-like quasiparticles at the same excitation energy $|\varepsilon|$. That is the quantity $\delta\dot{Q}(\varepsilon, x) + \delta\dot{Q}(-\varepsilon, x) \propto -\nabla F(\varepsilon, x)$, where we introduced $F(\varepsilon, x) \equiv f(\varepsilon, x) - f(-\varepsilon, x)$.

In the diffusive transport regime, within each NW segment the EED satisfies the equation $\frac{\partial^2}{\partial x^2} f(\varepsilon, x) = 0$ and interpolates linearly as a function of x between the boundary conditions [30]. Thus, the conservation of the heat flux is expressed as:

$$\begin{aligned} |\varepsilon| < \Delta : \\ \frac{F_1(\varepsilon) - F_L(\varepsilon)}{r_L} &= (F_2(\varepsilon) - F_1(\varepsilon)) \cdot G_{\text{th}} \\ \frac{F_R(\varepsilon) - F_2(\varepsilon)}{r_R} &= (F_2(\varepsilon) - F_1(\varepsilon)) \cdot G_{\text{th}}, \end{aligned} \quad (1)$$

where the functions $F_{L,R}$ are given by the equilibrium Fermi-Dirac EEDs $f_0(\varepsilon - \mu_{L,R})$ and functions $F_{1,2}$ correspond to the boundaries of the S segment at $x = x_1$

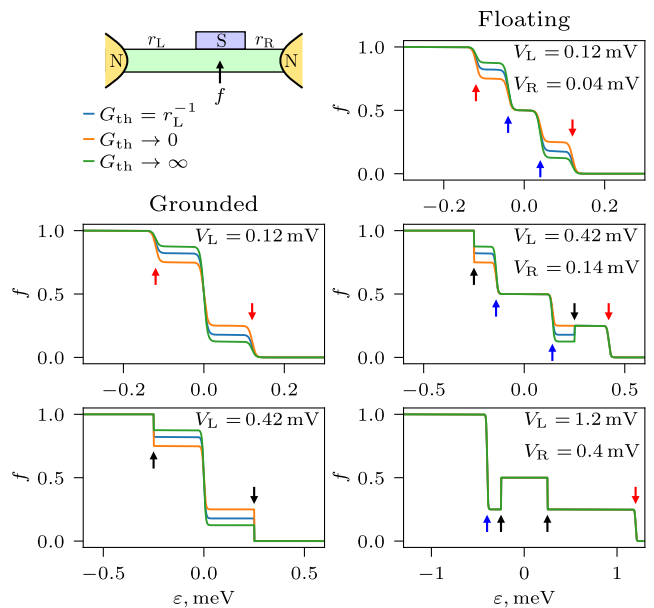


FIG. 2. The EED in middle of the S segment, $f \equiv (f_1 + f_2)/2$, at several applied biases. Arrows on the graphs denote specific energies: black arrow - Δ , red arrow - $|eV_L|$, blue arrow - $|eV_R|$. Resistances of the normal segments are the same as in Fig. 1, $T = 50$ mK.

and $x = x_2$. The solution of Eq. (1) is straightforward:

$$\begin{aligned} |\varepsilon| < \Delta : \\ f_1 &= \frac{1}{2} \left(1 + \frac{F_R r_L + F_L (r_R + 1/G_{\text{th}})}{r_L + 1/G_{\text{th}} + r_R} \right) \\ f_2 &= \frac{1}{2} \left(1 + \frac{F_L r_R + F_R (r_L + 1/G_{\text{th}})}{r_L + 1/G_{\text{th}} + r_R} \right). \end{aligned} \quad (2)$$

For above-gap energies $|\varepsilon| > \Delta$ we neglect the ARs and assume that the S segment essentially behaves as a piece of normal metal with the conductance much higher than that of the normal NW segments. Thus $f(\varepsilon)$ is independent of coordinate for $x \in [x_1, x_2]$. In the Grounded case the EED in the S segment is simply given by the equilibrium EED with $\mu = \mu_S \equiv 0$. In the Floating case the EED is calculated from matching the quasiparticle currents in the neighboring normal segments at $x = x_1$ and $x = x_2$ and acquires a familiar linear combination of the boundary conditions at the left and right N terminals [30]:

$$\begin{aligned} |\varepsilon| \geq \Delta : \\ f_{1,2} = \begin{cases} f_0, & \text{Grounded} \\ (f_R r_L + f_L r_R)/(r_L + r_R), & \text{Floating} \end{cases} \end{aligned} \quad (3)$$

It is straightforward to see that the Eqs. (2) and (3) contain a limiting case of a diffusive wire with N and S contacts. This situation is achieved for both device layouts taking $r_R = 0$ and $G_{\text{th}} = 0$. In this case the voltage

drop on the right N-section is zero, $\mu_R = 0$, and $f_2(\varepsilon)$ is given by the equilibrium EED. The energy distribution at $x = x_1$ has a well-known double-step shape [18] with $f_1(\varepsilon) = 1/2$ for $|\varepsilon| < \Delta$, $|eV|$ and 0 or 1 otherwise.

In general, the situation is more sophisticated. In Fig. 2 we plot the EED in the middle of S segment for both device layouts at different bias voltages assuming that the sub-gap thermal conductance is independent of energy. Different line styles correspond to three representative values of G_{th} , see the legend. The vertical arrows show the positions of the chemical potentials and the gap edges as explained in the caption. For small enough bias voltages the EED has three steps in the Grounded case and four steps in the Floating case (upper panels in both columns). These steps are smeared by the finite temperature. In addition, the step in $f(\varepsilon)$ occurs each time the voltage drop on one of the normal NW segments equals Δ , these steps at the gap edges are sharp. In the Grounded case $f(|\varepsilon| > \Delta)$ is equilibrium, see the Eq. (3) and the lower panel in the left column of Fig. 2. In the Floating case the situation is much richer and the EED may be non-monotonic and exhibit up to five steps depending on the relation between the voltage drops $V_{L,R}$ and the superconducting gap, see the lower two panels in the right column of Fig. 2. Note that such EEDs in the S segment can be directly measured with a local tunnel probe using transport [31] or noise [32] approaches.

IV. SHOT NOISE

Knowing the EEDs on the boundaries of the S segment (Eqs. (2, 3)) for the EED one finds the $f(\varepsilon, x)$ and the local noise temperature $T_N(x)$. The spectral density of the spontaneous current fluctuations in the normal segments of the NW is then calculated using the semiclassical solution for diffusive conductors [30]:

$$\begin{aligned} T_N(x) &= \frac{1}{k_B} \int_{-\infty}^{+\infty} f(\varepsilon, x)(1 - f(\varepsilon, x))d\varepsilon \\ S_L &= \frac{4k_B}{r_L} \int_{x_L}^{x_1} T_N(x)dx \\ S_R &= \frac{4k_B}{r_R} \int_{x_2}^{x_R} T_N(x)dx. \end{aligned} \quad (4)$$

A separate measurement of the fluctuations S_L and S_R is possible only in the Grounded case [33]. In the Floating case the normal segments are connected in series and the resulting current fluctuation is [34]:

$$S = \frac{S_L r_L^2 + S_R r_R^2}{(r_L + r_R)^2}.$$

Note that in the last equation the contribution of the S segment to the measured shot noise is absent thanks to its zero resistance. Nevertheless, the role of the thermal conductance in the S segment is decisive, since it is G_{th} that determines the non-equilibrium EEDs on the boundaries of S segment.

Grounded

Using the notations $\theta = [1 + G_{\text{th}}(r_L + r_R)]^{-1}$ and $\alpha = r_L/(r_L + r_R)$ we express the general solutions for the S_L and S_R in the Grounded case in the zero temperature limit as follows:

$$S_L = \frac{2e}{3r_L} \begin{cases} V(2 - (\alpha - \alpha\theta)^2), & V < \Delta \\ V + \Delta(1 - (\alpha - \alpha\theta)^2), & V \geq \Delta \end{cases} \quad (5)$$

$$S_R = \frac{2e}{3r_L} \Xi \begin{cases} V, & V < \Delta \\ \Delta, & V \geq \Delta \end{cases} \quad (6)$$

$$\Xi(\alpha, \theta) = \alpha(1 - \theta)(2 + \theta + \alpha(1 - \theta)).$$

Representative results for the shot noise spectral density are plotted in Fig. 3(a) and Fig. 3(b). Here, the G_{th} is energy independent and the correspondence between the line colours and the G_{th} values is shown on the nearby colour bar. Both current fluctuations S_L and S_R demonstrate a kink at $|eV| = \Delta$, when the voltage applied on the left N terminal meet the superconducting gap edge. The effect of finite sub-gap thermal conductance of the S segment on the S_L and S_R is different. The noise of the biased normal segment S_L is maximum if the thermal transport is suppressed and diminishes at increasing G_{th} . By contrast, the noise of the unbiased normal segment S_R , that originates from the quasiparticles transmitted via the proximity region, is only observable at $G_{\text{th}} > 0$. Note that S_R saturates at $|eV| > \Delta$, since above the gap the quasiparticles sink in the grounded S terminal.

Floating

Using the same notations, and assuming without the loss of generality that $\alpha \geq \frac{1}{2}$, we express the results for the shot noise in the Floating case as follows:

$$\begin{aligned} S &= \frac{2eV}{3R} \\ &+ \frac{2e}{3R} \Gamma \begin{cases} (2\alpha - 1)V, & \alpha V < \Delta \\ -(1 - \alpha)V + \Delta, & \text{else} \\ 0, & (1 - \alpha)V \geq \Delta \end{cases} \end{aligned} \quad (7)$$

$$\Gamma(\alpha, \theta) = 1 - 3\alpha^2(\theta - 1)\theta + \alpha(3\theta^2 - 1) - \theta(\theta + 1),$$

where $R = r_L + r_R$ is end-to-end resistance of the device.

Fig. 3(c) and Fig. 3(d) summarize the representative results in the Floating case. The key distinction here is the presence of two kinks on the bias dependence of the shot noise, each time the voltage drop on one of the sections corresponds to Δ (for the marginal case $r_R = 0$ the kink at $\Delta/(1 - \alpha)$ goes to infinity, see Fig. 3(d)). For the particular choice of $r_L : r_R = 4$ the kinks are observed at $|eV| = 5/4\Delta$ and at $|eV| = 5\Delta$, see Fig. 3(c). Below the second kink the noise is sensitive to the value of thermal

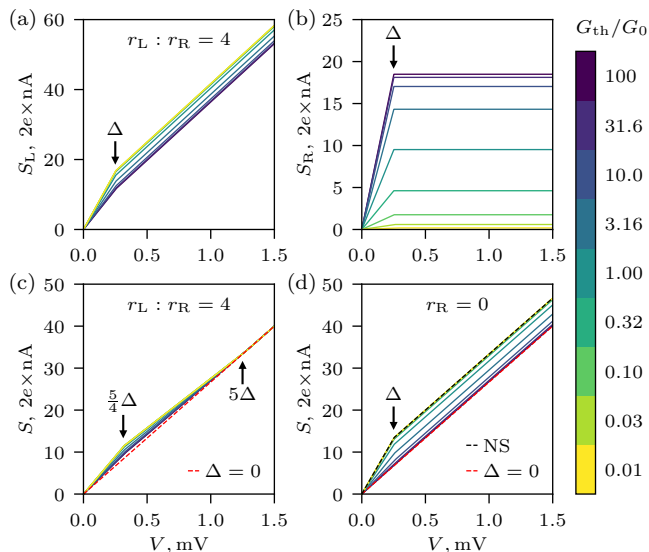


FIG. 3. Zero temperature shot noise evaluated at various G_{th} expressed in units of $G_0 = 2e^2/h$. (a-b) Current fluctuations of the biased (S_L) and unbiased (S_R) normal segments in the Grounded geometry, $r_L : r_R = 4$. (c-d) Current fluctuations in the Floating geometry, $r_L + r_R$ is kept constant in both panels. Red dashed are the guide lines for ordinary metallic diffusive wire, $F = 1/3$. Black dashed line represents the dirty NS junction without the sub-gap states [18]. In (a-c) the resistances of the normal segments are $r_L = 10 \text{ k}\Omega$ and $r_R = 2.5 \text{ k}\Omega$. In (d) $r_L = 12.5 \text{ k}\Omega$ and $r_R = 0$.

conductance and the sensitivity is maximum at the position of the first kink. Above the second kink the shot noise coincides with the universal value in metallic diffusive conductors [30] $S = 2eV/3R$ shown by the dashed line and does not display any signatures of the superconductivity. Of special interest in the Floating case is the situation of a fully antisymmetric device layout, that is the limit of $r_R = 0$, shown in Fig. 3(d). In this case the only kink is at the usual position $|eV| = \Delta$, and the $S(V)$ dependence shows the strongest dependence on G_{th} and interpolates between the well known limits in diffusive normal and NS cases depending on G_{th} . Note that in a symmetric Floating device layout ($\alpha = 1/2$) the measurement of the shot noise is useless since $S = 2eV/3R$ in the whole bias range independent of the G_{th} value.

V. ENERGY DEPENDENT THERMAL CONDUCTANCE

In previous sections we treated the problem for the energy independent thermal conductance. Thanks to the absence of the energy relaxation, however, the shot noise measurement provides access to a full energy dependence of $G_{\text{th}}(\varepsilon)$, which may result from the energy dependence of the quasiparticle density of states. This information is contained in a slope $\partial S/\partial I$ and is conveniently expressed

in terms of a renormalized effective charge e^* as follows:

$$\begin{aligned} &\text{Grounded:} \\ |eV| < \Delta: e^* &\equiv \frac{1}{2eF} \frac{\partial S_R}{\partial I_L} = \Xi(\alpha, \theta) \\ |eV| > \Delta: e^* &= 0 \end{aligned} \quad (8)$$

$$\begin{aligned} &\text{Floating, } r_R \rightarrow 0: \\ |eV| < \Delta: e^* &\equiv \frac{1}{2eF} \frac{\partial S}{\partial I} = 1 + \Gamma(1, \theta) \\ |eV| > \Delta: e^* &= 1, \end{aligned} \quad (9)$$

where $F = 1/3$ is the universal value of the Fano factor in metallic diffusive conductors. The energy dependence of the sub-gap thermal conductance enters the expression for the effective charge via $\theta(\varepsilon) = [1 + G_{\text{th}}(\varepsilon)(r_L + r_R)]^{-1}$. Similarly to the Grounded case (8), the limit $r_R \rightarrow 0$ ($\alpha = 1$) of the Floating case provides the direct relation between e^* and $G_{\text{th}}(eV)$ via expression (9). In contrast, a generic Floating case with $\alpha < 1$ is less convenient since the effective charge is dependent on both $G_{\text{th}}(\alpha eV)$ and $G_{\text{th}}(eV - \alpha eV)$. The corresponding bulky expressions for the e^* are offloaded to the Appendix B.

In the following we illustrate these results for the simplest realizations of $G_{\text{th}}(\varepsilon)$, see Fig. 4 (row i). $G_{\text{th}}(\varepsilon)$ is assumed to be a stepwise function:

$$G_{\text{th}}(\varepsilon) = \begin{cases} G_1, & |\varepsilon| < \Delta_1 \\ G_2, & \Delta_1 \leq |\varepsilon| < \Delta, \end{cases}$$

which imitates a one dimensional wire for the case of a topological phase transition $(G_1, G_2) = (2e^2/h, 0)$ [12] and for the case of a hard superconducting gap $(G_1, G_2) = (0, 2e^2/h)$ of width $\Delta_1 < \Delta$ [35, 36].

In Fig. 4 we plot the bias dependencies of the shot noise and e^* for these two situations, respectively, in column (a) and column (b). Here, $r_L = 10 \text{ k}\Omega$ and $r_R \rightarrow 0$. For both device layouts the shot noise spectral density shows a kink each time the G_{th} changes abruptly. Consequently, the shape of the bias dependence of the e^* mimics the energy dependence of the thermal conductance, cf. the panels (ii) and (iii) with the corresponding panels (i) in Fig. 4. Two key differences between the Grounded and Floating cases are evident. First, in the Grounded case the e^* increases as function of G_{th} , whereas in the Floating case the dependence is opposite. Second, in the Grounded case the effective charge varies between 0 and 3, $e^* = 0$ corresponding to $G_{\text{th}} = 0$, whereas in the Floating case $1 \leq e^* \leq 2$, $e^* = 2$ corresponding to $G_{\text{th}} = 0$.

VI. CONCLUSION

We analyzed how a finite sub-gap thermal conductance of a superconducting proximity region is manifested in

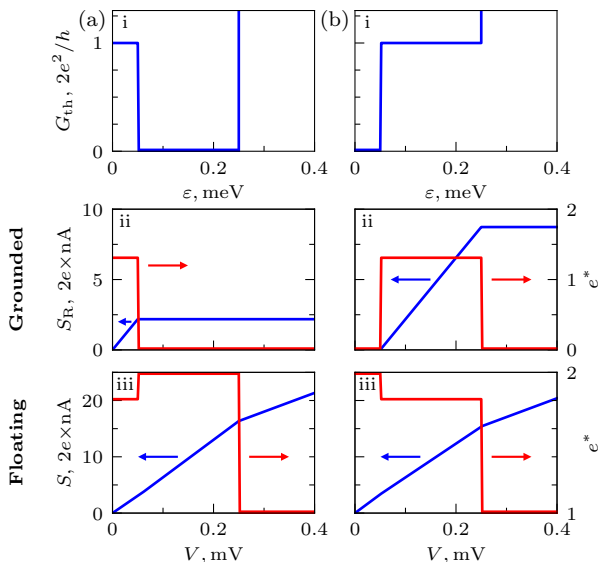


FIG. 4. Measurement of energy dependent $G_{\text{th}}(\varepsilon)$ via shot noise. (i) Stepwise $G_{\text{th}}(\varepsilon)$ functions imitating the (a) topological phase transition and (b) hard gap $\Delta_1 = 50 \mu\text{eV}$. (ii) Current fluctuations of the unbiased segment and e^* in the Grounded setup. (iii) Current fluctuations and e^* in the Floating setup.

the shot noise of diffusive NSN structures. Two possible device layouts — three-terminal with a grounded super-

conducting island and two-terminal with a floating superconducting island — permit a direct measurement of the energy dependence $G_{\text{th}}(\varepsilon)$ from the bias dependence of the shot noise. The Floating case may be attractive for the experimental realization in semiconducting nanowires with a thin superconducting shell that maybe technically challenging to contact. In this case the device asymmetry is crucial in the shot noise experiment, that can be engineered by means of the structure design and/or local gating. Applicable to diffusive multi-mode wire structures our results may also serve as a qualitative starting point to understand the shot noise response in open one dimensional Majorana devices.

VII. ACKNOWLEDGMENTS

We thank A.O. Denisov, K.E. Nagaev and, particularly, E.S. Tikhonov for valuable discussions. This work was mainly supported by the RSF project 19-12-00326. The calculation of the finite temperature shot noise expression in Appendix A was performed under the state task of ISSP RAS.

APPENDIX A: THE GROUNDED GEOMETRY. FINITE TEMPERATURE

Here we provide the finite temperature expression for shot noise of the unbiased normal segment in the Grounded geometry. We use $e, k_B = 1, \gamma = r_R / (r_L + r_R + 1/G_{\text{th}})$.

$$S_R = \frac{4T}{r_R} + \frac{2T}{3r_R} \gamma \left\{ \left[\gamma + 3(2 - \gamma) \coth^2 \left(\frac{V}{2T} \right) \right] \tanh \left(\frac{V}{2T} \right) \operatorname{artanh} \left[\tanh \left(\frac{\Delta}{2T} \right) \tanh \left(\frac{V}{2T} \right) \right] + \frac{1}{2} \left[\gamma - 3(2 - \gamma) \cosh \left(\frac{\Delta}{T} \right) - 2(3 - \gamma) \cosh \left(\frac{V}{T} \right) \right] \tanh \left(\frac{\Delta}{2T} \right) \operatorname{sech} \left(\frac{V - \Delta}{2T} \right) \operatorname{sech} \left(\frac{\Delta + V}{2T} \right) \right\}$$

APPENDIX B: GENERAL RESULT IN THE FLOATING GEOMETRY

In the general case (arbitrary r_L, r_R and energy dependent $G_{\text{th}}(\varepsilon)$) shot noise in the Floating layout exhibits 2 kinks (see Fig. 3(c)). Here we write the expression for e^* defined in Eq. (9), where θ contains $G_{\text{th}}(\varepsilon)$.

$$e^* = \begin{cases} \alpha(1 - \alpha) + \alpha(3\alpha^2 - 1)\theta(\alpha V) - \alpha(3\alpha^2 - 3\alpha + 1)\theta^2(\alpha V) + \\ \alpha(2 - \alpha) + (3\alpha^3 - 3\alpha^2 - \alpha + 1)\theta(V(1 - \alpha)) + (-3\alpha^3 + 6\alpha^2 - 4\alpha + 1)\theta^2(V(1 - \alpha)), & \alpha V < \Delta \\ \alpha(2 - \alpha) + (3\alpha^3 - 3\alpha^2 - \alpha + 1)\theta(V(1 - \alpha)) + (-3\alpha^3 + 6\alpha^2 - 4\alpha + 1)\theta^2(V(1 - \alpha)), & \text{else} \\ 1, & (1 - \alpha)V \geq \Delta \end{cases}$$

- [1] R. M. Lutchyn, J. D. Sau, and S. Das Sarma, *Phys. Rev. Lett.* **105**, 077001 (2010).
- [2] Y. Oreg, G. Refael, and F. von Oppen, *Phys. Rev. Lett.* **105**, 177002 (2010).
- [3] J. Alicea, *Rep. Prog. Phys.* **75**, 076501 (2012).
- [4] Ö. Gül, H. Zhang, J. D. S. Bommer, M. W. A. de Moor, D. Car, S. R. Plissard, E. P. A. M. Bakkers, A. Geresdi, K. Watanabe, T. Taniguchi, and L. P. Kouwenhoven, *Nature Nanotechnology* **13**, 192 (2018).
- [5] V. Mourik, K. Zuo, S. M. Frolov, S. R. Plissard, E. P. a. M. Bakkers, and L. P. Kouwenhoven, *Science* **336**, 1003 (2012).
- [6] P. Krogstrup, N. L. B. Ziino, W. Chang, S. M. Albrecht, M. H. Madsen, E. Johnson, J. Nygård, C. M. Marcus, and T. S. Jespersen, *Nature Materials* **14**, 400 (2015).
- [7] G. C. Ménard, G. L. R. Anselmetti, E. A. Martinez, D. Puglia, F. K. Malinowski, J. S. Lee, S. Choi, M. Pendharkar, C. J. Palmstrøm, K. Flensberg, C. M. Marcus, L. Casparis, and A. P. Higginbotham, *Phys. Rev. Lett.* **124**, 036802 (2020).
- [8] D. Puglia, E. A. Martinez, G. C. Ménard, A. Pöschl, S. Gronin, G. C. Gardner, R. Kallaher, M. J. Manfra, C. M. Marcus, A. P. Higginbotham, and L. Casparis, [arXiv:2006.01275](https://arxiv.org/abs/2006.01275) (2020).
- [9] P. Yu, J. Chen, M. Gomanko, G. Badawy, E. P. a. M. Bakkers, K. Zuo, V. Mourik, and S. M. Frolov, *Nature Physics* , 1 (2021).
- [10] Y.-H. Lai, J. D. Sau, and S. Das Sarma, *Phys. Rev. B* **100**, 045302 (2019).
- [11] T. Ö. Rosdahl, A. Vuik, M. Kjaergaard, and A. R. Akhmerov, *Phys. Rev. B* **97**, 045421 (2018).
- [12] A. R. Akhmerov, J. P. Dahlhaus, F. Hassler, M. Wimmer, and C. W. J. Beenakker, *Phys. Rev. Lett.* **106**, 057001 (2011).
- [13] H. Pan, J. D. Sau, and S. Das Sarma, *Phys. Rev. B* **103**, 014513 (2021).
- [14] L. Fu, *Phys. Rev. Lett.* **104**, 056402 (2010).
- [15] J. Ulrich and F. Hassler, *Phys. Rev. B* **92**, 075443 (2015).
- [16] X. Jehl, M. Sanquer, R. Calemczuk, and D. Maily, *Nature* **405**, 50 (2000).
- [17] A. A. Kozhevnikov, R. J. Schoelkopf, L. E. Calvet, M. J. Rooks, and D. E. Prober, *Journal of Low Temperature Physics* **118**, 671 (2000).
- [18] K. E. Nagaev and M. Büttiker, *Phys. Rev. B* **63**, 081301 (2001).
- [19] K. E. Nagaev, *Phys. Rev. B* **64**, 081304 (2001).
- [20] E. S. Tikhonov, D. V. Shovkun, M. Snelder, M. P. Stehno, Y. Huang, M. S. Golden, A. A. Golubov, A. Brinkman, and V. S. Khrapai, *Phys. Rev. Lett.* **117**, 147001 (2016).
- [21] M. R. Sahu, A. K. Paul, A. Soori, K. Watanabe, T. Taniguchi, S. Mukerjee, and A. Das, *Phys. Rev. B* **100**, 235414 (2019).
- [22] A. O. Denisov, A. V. Bubis, S. U. Piatrusha, N. A. Titova, A. G. Nasibulin, J. Becker, J. Treu, D. Ruhstorfer, G. Koblmüller, E. S. Tikhonov, and V. S. Khrapai, [arXiv:2101.02128](https://arxiv.org/abs/2101.02128) (2021).
- [23] N. B. Kopnin, A. S. Mel'nikov, and V. M. Vinokur, *Phys. Rev. B* **70**, 075310 (2004).
- [24] A. F. Andreev, *Sov. Phys. JETP* **19**, 1228 (1964).
- [25] A. F. Andreev, *Sov. Phys. JETP* **20**, 1490 (1965).
- [26] S. Gazibegovic, D. Car, H. Zhang, S. C. Balk, J. A. Logan, M. W. A. de Moor, M. C. Cassidy, R. Schmits, D. Xu, G. Wang, P. Krogstrup, R. L. M. Op het Veld, K. Zuo, Y. Vos, J. Shen, D. Bouman, B. Shojaei, D. Pennachio, J. S. Lee, P. J. van Veldhoven, S. Koelling, M. A. Verheijen, L. P. Kouwenhoven, C. J. Palmstrøm, and E. P. A. M. Bakkers, *Nature* **548**, 434 (2017).
- [27] F. Krizek, J. E. Sestoft, P. Aseev, S. Marti-Sanchez, S. Vaitiekėnas, L. Casparis, S. A. Khan, Y. Liu, T. Stankevič, A. M. Whiticar, A. Fursina, F. Boekhout, R. Koops, E. Uccelli, L. P. Kouwenhoven, C. M. Marcus, J. Arbiol, and P. Krogstrup, *Phys. Rev. Materials* **2**, 093401 (2018).
- [28] S. Vaitiekėnas, A. M. Whiticar, M.-T. Deng, F. Krizek, J. E. Sestoft, C. J. Palmstrøm, S. Marti-Sanchez, J. Arbiol, P. Krogstrup, L. Casparis, and C. M. Marcus, *Phys. Rev. Lett.* **121**, 147701 (2018).
- [29] N. S. Kirsanov, Z. B. Tan, D. S. Golubev, P. J. Hakonen, and G. B. Lesovik, *Phys. Rev. B* **99**, 115127 (2019).
- [30] K. Nagaev, *Phys Lett A* **169**, 103 (1992).
- [31] H. Pothier, S. Guéron, N. O. Birge, D. Esteve, and M. H. Devoret, *Phys. Rev. Lett.* **79**, 3490 (1997).
- [32] E. S. Tikhonov, A. O. Denisov, S. U. Piatrusha, I. N. Khrapach, J. P. Pekola, B. Karimi, R. N. Jabdaraghi, and V. S. Khrapai, *Phys. Rev. B* **102**, 085417 (2020).
- [33] A. O. Denisov, A. V. Bubis, S. U. Piatrusha, N. A. Titova, A. G. Nasibulin, J. Becker, J. Treu, D. Ruhstorfer, G. Koblmüller, E. S. Tikhonov, and V. S. Khrapai, [arXiv:2006.09803](https://arxiv.org/abs/2006.09803) (2020).
- [34] C. W. J. Beenakker and M. Büttiker, *Phys. Rev. B* **46**, 1889 (1992).
- [35] W. Chang, S. M. Albrecht, T. S. Jespersen, F. Kuemmeth, P. Krogstrup, J. Nygård, and C. M. Marcus, *Nature Nanotech* **10**, 232 (2015).
- [36] M. Kjaergaard, F. Nichele, H. J. Suominen, M. P. Nowak, M. Wimmer, A. R. Akhmerov, J. A. Folk, K. Flensberg, J. Shabani, C. J. Palmstrøm, and C. M. Marcus, *Nat Commun* **7**, 12841 (2016).